Organic/Inorganic Imide Nanocomposites from Aminophenylsilsesquioxanes

Jiwon Choi, Ryo Tamaki,† Seung Gyoo Kim, and Richard M. Laine*

Macromolecular Science and Engineering Center and the Department of Materials Science and Engineering, University of Michigan, Ann Arbor, Michigan 48109-2136

Received March 11, 2003. Revised Manuscript Received June 12, 2003

We present here part of an ongoing study on structure−processing−property relationships in cubic silsesquioxane (cube) nanocomposites. Here, we focus on imide nanocomposites prepared from octaaminophenylsilsesquioxane (OAPS) as a model nanobuilding block for rigid, high-temperature hybrid nanocomposite materials. OAPS units are linked NH_2 vertex to NH_2 vertex by reaction with various dianhydrides to form three-dimensional nanocomposites. The architecture of the organic tethers between vertices can be manipulated to optimize processability, rigidity, and thermomechanical properties. Studies were initiated using an extreme tether structure with zero flexibility prepared by solvent casting and then curing mixtures of OAPS with pyromellitic dianhydride (PMDA) at 330 °C. The resulting materials are extremely brittle, making thermomechanical property measurements quite difficult. Tether rigidity, length, and cross-link densities were then modified using reactions of OAPS with oxydiphthalic anhydride (ODPA) and diluting with oxydianiline (ODA) to adjust nanocomposite stiffness. FTIR and DMA of the OAPS/ODPA/ODA nanocomposites suggest that cure temperatures of >500 °C are necessary for optimal imidization. However, increasing the cross-link density alone by increasing OAPS loading without curing at high temperatures also significantly improves thermomechanical stabilities. DMA, TGA, and nanoindentation measurements show that macroscopic relaxation is eliminated completely at OAPS loadings of >60 mol % providing 5% mass loss at temperatures >570 °C and compressive moduli of ≈3.8 GPa.

Introduction

Organic/inorganic hybrid nanocomposites represent a new frontier in materials chemistry, science, and engineering because they offer the potential to develop and tailor materials with control at the finest length scales.[1−16] This in turn could lead to materials with novel properties engendered by both the length scales involved and the potential for multifunctionality. However, in developing such hybrid nanocomposites, the ability to predict and tailor properties must rely on an understanding of nanoscale structure−processing−property relationships such that components can be custom-designed and processed properly to achieve target properties. Although significant advances have been made in developing nanocomposites, the systematic study of the effects of variations in nanocomponent architecture, processing, and final nanostructure on macroscopic properties leading to a fundamental understanding of the various relationships remains a considerable challenge.

A logical approach to such studies is to create well-defined model systems wherein multiple parameters can be varied selectively and their effects on macroscopic properties can be mapped. To this end, we have begun to delineate structure−processing−property relationships in cubic silsesquioxane (Figure 1) nanocomposites.[17−23] These "nanobuilding blocks" (0.53-nm body diagonal) provide an excellent mechanism for combining organic/inorganic components at the nanoscale.[14−16] The cubes represent invariant nano-reinforcing components covalently connected by organic tethers (R = 1∼2 nm depending on structure) between cube vertices. Thus, the sizes and periodicity of the inorganic and organic

* To whom correspondence should be addressed. Phone: 734-764-6203. E-mail: talsdad@umich.edu.
† Currently at Tyco Electronics Corporation, Technology Division, Menlo Park, CA 94025.

(1) (a) Sanchez, C.; Lebeau, B. *MRS Bull.* **2000**, *26*, 377. (b) Rajeshwar, K.; de Tacconi, N. R.; Chenthamarakshan, C. R. *Chem. Mater.* **2001**, *13*, 2765.
(2) Gomez-Romero, P. *Adv. Mater.* **2001**, *13*, 163.
(3) Seraji, S.; Wu, Y.; Forbes, M.; Limmer, S. J. Chou, T.; Cao, G. *Adv. Mater.* **2000**, *12*, 1695.
(4) Matejka, L.; Dukh, O. *Macromol. Symp.* **2001**, *171*, 181.
(5) Alexandre, M.; Dubois, P. *Mater. Sci. Eng.* **2000**, *28*, 1.
(6) LeBaron, P. C., Wang, Z.; Pinnavaia, T. J. *Appl. Clay Sci.* **1999**, *15*, 11.
(7) Vaia, R. A.; Price, G.; Ruth, P. N.; Nguyen, H. T.; Lichtenhan, J. *Appl. Clay Sci.* **1999**, *15*, 67.
(8) Tsai, M.; Whang, W.-T. *Polymer* **2001**, *42*, 4197.
(9) Lan, J. K.; Wang, Y. L.; Wu, Y. L.; Liou, H. C.; Wang, J. K.; Chiu, S. Y.; Cheng, Y. L.; Feng, M. S. *Thin Solid Films* **2000**, *377−378*, 776.
(10) Harkness, B. R.; Takeuchi, K.; Tachikawa, M. *Macromol.* **1998**, *31*, 4798.
(11) Rottman, C.; Grader, G.; DeHazan, Y.; Melchior, S. Avnir, D. *J. Am. Chem. Soc.* **1999**, *121*, 8533.
(12) Wirnsberger, G.; Scoott, B. J.; Chmelka, B. F.; Stucky, G. D. *Adv. Mater.* **2000**, *12*, 1450.
(13) Dantas De Morais, T.; Chaput, F.; Boilot, J.-P.; Lahlil, K.; Darracq, B.; Levy, Y. *Adv. Mater.* **1999**, *11*, 107.
(14) Sanchez, C.; Soler-Illia, G. J. de A. A.; Ribot, F.; Lalot, T.; Mayer, C. R.; Cabuil, V. *Chem. Mater.* **2001**, *13*, 3061.
(15) Pyun, J.; Matyjaszewki, K. *Chem. Mater.* **2001**, *13*, 3436.
(16) Schubert, U. *Chem. Mater.* **2001**, 13, 3487.

10.1021/cm030286h CCC: $25.00
Published on Web 07/23/2003

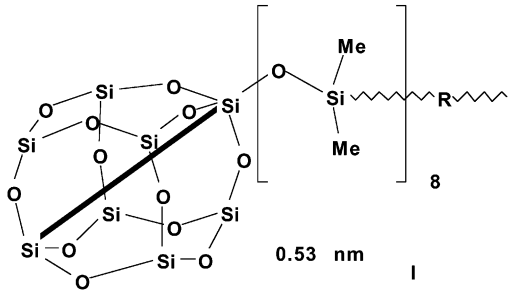

Figure 1. Generic octadimethylsiloxysilsesquioxane (**I**) nanocomposite building block.

domains upon cross-linking can be exactly defined. Network parameters including tether architecture (e.g., rigidity), length, and cross-link density can then be varied systematically, and the associated global properties can be characterized as a function of these changes.

Equally important, this approach also offers the opportunity to predict and tailor macroscopic properties because it offers control of chemical and physical structures at the nanoscale by virtue of using octafunctionally symmetrical building blocks typically 1−2 nm in diameter. Assuming complete control of the reactions that form vertex to vertex interconnects (tethers, see Scheme 1), their assembly should provide exceptional control of macroscopic behavior.

The type of nanocomposite shown in Scheme 1 is one that is completely discontinuous. That is, organic tethers couple only with cube vertices and not with each other. These types of nanocomposites isolate the organic components from each other. Therefore, transmission of mechanical load must be between components. Thus, thermomechanical properties studies will probe both components simultaneously. Given the nature of the cube, the properties measured are expected to arise primarily from the organic tether nanoarchitecture.

An additional outcome of these types of studies concerns the behavior of the tethers themselves. Because of their size, rigidity, multiple cross-links, and bulk, cubes will greatly limit the cooperative motion of multiple tethers. Therefore, the opportunity exists to study the behavior of isolated tether segmental motions free of chain contributions found in linear or even partially cross-linked polymers.

The first step in the overall process was to develop synthesis techniques to append various functional groups to cubes that could in turn be covalently coupled to form well-defined networks, as discussed elsewhere.[19] The functional groups and coupling processes were chosen to generate nanocomposites where both components are uniformly and periodically distributed at the nanometer scale, and discontinuous. Epoxy resin cube nanocomposite studies[17,18,23] provided protocols for the systematic construction/analysis of hybrid networks and property characterization. From these, several basic nanostructure−processing−property relationships were identified, as expected: (1) tether properties (e.g., flexibility and thermal stability) strongly influence nanocomposite thermomechanical properties, (2) simple modification of tether architecture and the cross-link density can strongly influence the macroscopic properties of these nanocomposites, and (3) the thermal stability of aliphatic tether sections is a limiting factor.

Consequently, we sought nanobuilding blocks without aliphatic content resulting in the development of octaaminophenylsilsesquioxane (octaanilino), (OAPS).[19] OAPS offers access to nanocomposite epoxy resins,[23] but more importantly to aliphatic free amides and imides.[22] In particular, polyimides, because of their widespread commercial importance ranging from structural materials (fibers) to electronic substrates, represent an attractive synthetic target with practical implications. As with the epoxy resin studies, model studies were undertaken beginning with the synthesis of the octaphthalimide followed by the polyimide illustrated in Scheme 1.[22]

The Scheme 1 product represents the prototypical nanocomposite imide. The short, planar, and aromatic character of the pyromellitic diimide tethers provides an extreme in tether rigidity offering no flexibility whatsoever except where defects remain from the imidization process. Indeed, the Scheme 1 imidization process requires severe conditions relative to normal polyimidization and is nearly complete only at temperatures of 550 °C. The resulting material is so brittle that mechanical properties measurements were not possible as all cast samples fractured during the curing process. The efforts discussed below use a slightly more flexible tether forming reactant, oxydiphthalic anhydride (ODPA)

Scheme 1. Reaction of OAPS with Pyromellitic Anhydride (PMDA) To Form a Nanocomposite with Completely Rigid Imide Tethers between Cube Vertices: Cure Temperatures of >300 °C Are Required To Obtain Optimal Cross-Linking[22]

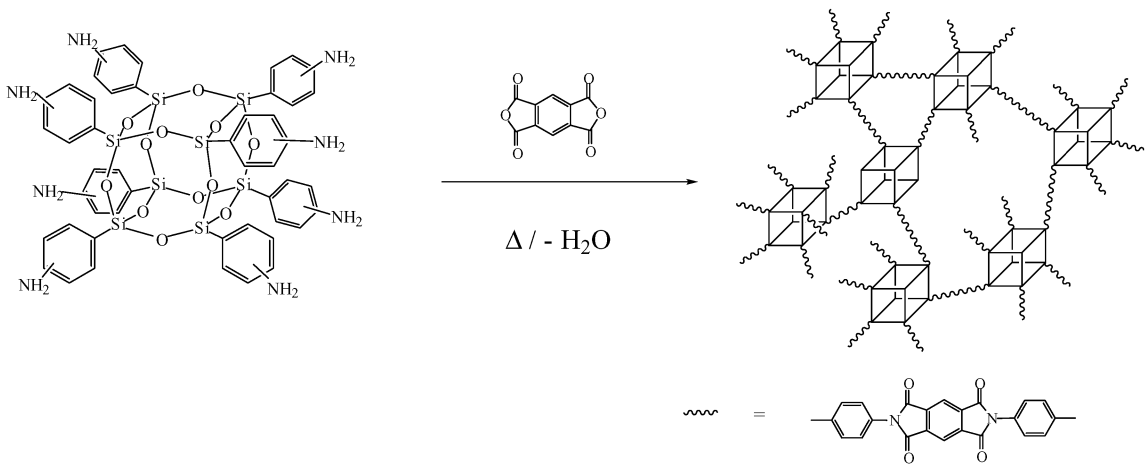

as the dianhydride, and oxydianiline (ODA) as a diluent, with the objective of developing structure−property relationships in OAPS-based polyimides with high compressive strengths and thermal stabilities.

Besides opportunities for structure−property relationship studies, imide cube nanocomposites also offer potential for novel properties. For example, given that silicon-containing polyimides show excellent resistance to atomic oxygen erosion in near-earth orbit environments,[24,25] imide cube nanocomposites may offer superior barrier properties vs organic imides because of the uniformly distributed cubes and the extra stability from cross-linking. Additionally, hydrophobic nanocomposites could minimize water uptake significantly, a source of polyimide degradation in applications such as interlayer dielectrics or protective coatings in integrated circuits.[26−31] Our preliminary studies show that water uptake in epoxy nanocomposites prepared from epoxy-functionalized cubes is significantly lower than that in common epoxy resins.[32] Thus, imide cube nanocomposites are also likely to exhibit lower water uptake and thus less property degradation than organic polyimides. Furthermore, in comparison with polyimides hybridized via sol−gel methods[33−40] or reinforced with clays,[41−45] incorporating OAPS requires no additional process steps for hybridization.

Experimental Section

Materials. Pyromellitic dianhydride (PMDA, MW 218.1), 4,4′-oxydianiline (ODA, MW 200.2), 4,4′-oxydiphthalic anhydride (ODPA, MW 310.2), and *N*-methylpyrrolidinone (NMP) were purchased from Aldrich (Milwaukee, WI) and used without further purification. Octaaminophenylsilsesquioxane (OAPS, MW ≈ 1153) was synthesized following methods described in the literature and has a substitution pattern consisting of a 60:30:10 *m*/*o*/*p* mixture.[19]

Table 1. Formulation of OAPS/ODA/ODPA Imide Composites

	mol % OAPS in amine				
	0	20	40	60	100
ODPA(g)[a]	0.310	0.310	0.310	0.310	0.310
OAPS(g)	0	0.058	0.115	0.173	0.288
ODA(g)	0.200	0.160	0.120	0.080	0

[a] Moles of anhydride kept at 2.00 mmol. Thus, total moles of amine in OAPS and ODA were also 2.00 mmol.

Nanocomposite Processing. *OAPS/PDMA Imides.* Nanocomposites were prepared using OAPS and PDMA. The mole ratio of anhydride/amine groups was kept at 1:1. OAPS (0.288 g, 0.25 mmol) and PDMA (0.218 g, 1.00 mmol) were dissolved separately in 5 mL of *N*-methylpyrrolidinone (NMP) in 20-mL glass vials. The two solutions were mixed at room temperature and shaken well by hand. The final solution was cast on a glass slide placed on a flat plate previously leveled and then dried for 12 h at room temperature and another 12 h at 60 °C in air. The prepared film was then heated under N_2 at 60 °C/h to 330 °C and kept at temperature for 3 h. The resulting thin film imide composites delaminated in small pieces due to extreme brittleness. These pieces were collected and analyzed by TGA.

OAPS/ODA/ODPA Imides. Nanocomposites with modified tether lengths and rigidity were prepared using OAPS, ODA, and ODPA. In formulating, the anhydride/amine group mole ratio was kept at 1:1. The mole ratio of OAPS/ODA was varied from 0 to 100 mol % of the amine portion. Table 1 shows the composite formulations.

OAPS/ODA/ODPA imide composites were prepared following the method described above. The resulting films were yellow-to-brown and transparent. The films (on the slides) were cut into 5−6 mm wide strips using a new razor blade. They were then immersed in cold water and sonicated for up to 1 h. The films were then easily removed from the substrates. The free-standing films were air-dried for 1 d and kept in a desiccator for TGA and DMA runs. Film thicknesses were 30−40 μm.

ODPA/ODA imide (0 mol % OAPS) was prepared separately following traditional methods,[33−45] which included preheating amic acid solutions before casting to increase the molecular weights to optimize properties. Thus, equimolar quantities of ODPA and ODA were dissolved together in 5 mL of *N*-methylpyrrolidinone (NMP) in 20-mL glass vials and preheated at ∼100 °C for 1 d. Film casting, curing, and retrieval from substrates were conducted as described above.

Characterization. *Fourier Transform Infrared Spectroscopy (FTIR) of Monomers.* Diffuse reflectance IR spectra (DRIFTS) were obtained on monomer powders using a Mattson Galaxy Series FTIR 3000 spectrometer (Mattson Instruments, Inc.). Optical-grade potassium bromide (KBr, International Crystal Laboratories, Garfield, NJ) was used as a background material. Cured sample (5 mg) and KBr crystal (500 mg) were ground together using an alumina mortar and pestle. The ground powder was packed into a sample holder and leveled off with a glass plate to give a smooth surface. The holder was placed in the sample chamber and the spectrum was recorded under dry N_2 purge. At least 128 scans were averaged for each spectrum. The resolution was ±4 cm^{-1}.

FTIR of Nanocomposite Films. Attenuated total reflection IR spectra (ATR) were obtained on the nanocomposite films using a Nexus 670 FTIR spectrometer (Nicolet). Background

(17) Laine, R. M.; Choi, J.; Lee, I. *Adv. Mater.* **2001**, *13*, 800.
(18) Choi, J.; Harcup, J.; Yee, A. F.; Zhu, Q.; Laine, R. M. *J. Am. Chem. Soc.* **2001**, *123*, 11420.
(19) Tamaki, R.; Tanaka, Y.; Asuncion, M. Z.; Choi, J.; Laine, R. M. *J. Am. Chem. Soc.* **2001**, *123*, 12416.
(20) Zhang, C.; Babonneau, F.; Bonhomme, C.; Laine, R. M.; Soles, C. L.; Hristov, H. A.; Yee, A. F. *J. Am. Chem. Soc.* **1998**, *120*, 8380.
(21) Zhang, C.; Laine, R. M. *J. Am. Chem. Soc.* **2000**, *122*, 6979.
(22) Tamaki, R.; Choi, J.; Laine, R. M. " *Chem. Mater.* **2003**, *15* (3), 793−797.
(23) (a) Choi, J.; Lee, I.; Yee, A. F.; Laine, R. M. "Organic/inorganic hybrid composites from cubic silsesquioxanes II", in preparation. (b) Choi, J.; Kim, S.; Tamaki, R.; Laine, R. M. "Organic/inorganic hybrid epoxy composites from aminophenylsilsesquioxane," in preparation.
(24) Feger, C.; Franke, H. In *Polyimides*, Ghosh, M. K., Mittal, K. L., Eds.; Marcel Dekker: New York, 1996; p 795.
(25) Neogi, S.; Gulino, D. A. *AlcheE J.* **1992**, *38*, 1379.
(26) Day, D. R. In *Polyimides: Materials, Chemistry and Characterization*; Feger, C., Khojasteh, M. M., McGrath, J. E., Eds.; Elsevier: Amsterdam, The Netherlands, 1989; p 537.
(27) Melcher, J.; Daben, Y.; Arlt, G. *IEEE Trans. Electron. Insul.* **1989**, *24*, 31.
(28) Numata, X.; Kinjo, N. *Polym. Eng. Sci.* **1988**, *28*, 906.
(29) Chung, I.; Park, C.; Ree, M.; Kim, S. *Chem. Mater.* **2001**, *13*, 2801.
(30) Van Alsten, J. G.; Coburn, J. C. *Macromolecules* **1994**, *27*, 3746.
(31) Tohge, N.; Tadanaga, K.; Sakatani, H.; Minami, T. *J. Mater. Sci. Lett.* **1996**, *15*, 1517.
(32) Choi, J.; Yee, A. F.; Laine, R. M. unpublished work.
(33) Wu, K. H.; Chang, T. C.; Yang, J. C.; Chen, H. B. *J. Appl. Polym. Sci.* **2001**, *79*, 965.
(34) Furukawa, N.; Yuasa, M.; Kimura, Y. *Polymer* **1999**, *40*, 1853.
(35) Chang, C. C.; Chen, W. C. *Chem. Mater.* **2002**, *14*, 4242.
(36) Chen, Y.; Iroh, J. O. *Chem. Mater.* **1999**, *11*, 1218.
(37) Huang, J.-C.; Zhu, Z.-K.; Yin, J.; Zhang, D.-M.; Qian, X.-F. *J. Appl. Polym. Sci.* **2001** *79*, 794.
(38) Hsiue, G.-H.; Chen, J.-K.; Liu, Y.-L. *J. Appl. Polym. Sci.* **2000**, *76*, 1609.
(39) Zhu, Z.; Yang, Y.; Yin, J.; Qi, Z. *J. Appl. Polym. Sci.* **1999**, *73*, 2977.
(40) Zju, Z.; Yin, J.; Cao, F.; Shang, X.; Lu, Q. *Adv. Mater.* **2000**, *12*, 1055.
(41) Agag, T.; Koga, T.; Takeichi, T. *Polymer* **2001**, *42*, 3399.
(42) Gu, A.; Kuo, S.; Chang, F. *J. Appl. Polym. Sci.* **2001**, *79*, 1902.
(43) Kim, G.-M.; Lee, D.-H.; Hoffmann, B.; Kressler, J.; Stoppelmann, G. *Polymer* **2001**, *42*, 1095.
(44) Yano, K.; Usuki, A.; Okada, A. *J. Polym. Sci. Part A: Polym. Chem.* **1997**, *35*, 2289.
(45) Lan, T.; Pinnavaia, T. J. *Chem. Mater.* **1994**, *6*, 2216.

scans in air were recorded prior to each measurement. Films were mounted on the Nicolet OMNI-Sampler with a constant pressure with a grip. The spectra were then averaged, using 128 scans in air. The resolution was ± 4 cm^{-1}.

Dynamic Mechanical Analysis (DMA). Dynamic mechanical behavior of imide films was studied using a TA instruments 2980 dynamic mechanical analyzer (New Castle, DE). Films previously cut into 5−6-mm strips were mounted in a tensile test clamp. Thicknesses were 30−40 μm with lengths of ~20 mm. Mechanical properties were measured under N_2 in step mode every 10 °C from 20 to 500 °C. Prior to each measurement, the environment was kept at the setting temperature for 10 min to ensure thermal equilibration. A frequency of 1 Hz was used for all measurements.

Thermal Gravimetric Analysis (TGA). Thermal stabilities of materials under N_2 or air were tested using a 2960 simultaneous DTA-TGA Instrument (TA Instruments, Inc., New Castle, DE). Samples (5−10 mg) were loaded in platinum pans and ramped to 1000 °C (10 °C/min/N_2). The N_2 or air flow rate was 60 mL/min.

Nanoindentation. Elastic moduli were measured using a Nano II Nanoindenter with a Berkovich tip. The area function of the diamond tip and the load frame stiffness were calibrated using a silica standard. A maximum load of 0.3 mN with a load rate of 0.03 mN/s was used. The penetration depth was about 200 nm. Loading and unloading were repeated three times, and a 100-s hold segment at 10% of the peak load was inserted after the third unloading to correct the rate of displacement produced by thermal expansion of the system.

Results and Discussion

The work reported here has several practical goals in addition to mapping structure−processing−property relationships. The first is to develop cube nanocomposites with very rigid tethers that can be expected to have very low coefficients of thermal expansion offering the potential for electronic substrate applications. The second is to develop materials that offer good-to-excellent compressive strengths, a property currently lacking in commercial polyaramid fibers. The third is to develop baseline mechanical properties data based on our longer term goal of creating systems that permit melt spinning of polyimide fiber nanocomposites without need of solvents.

As noted above, our first efforts to prepare polyimide nanocomposites explored the reaction of pyromellitic dianhydride (PMDA) with OAPS to produce materials with extremely short, rigid aromatic imide tethers.[22] However, no samples of sufficient quality for DMA measurements resulted from cast films cured to >300°C (see below). This led to efforts to introduce a slightly more flexible tether using oxydiphthalic anhydride (ODPA). As an additional measure, oxydianiline (ODA) was used as a diluent to reduce the overall cross-link density. The curing process and mechanical properties of a series of materials made with combinations of OAPS, ODA, and ODPA were then explored. FTIR was used to monitor cure behavior, and various properties were characterized using TGA, DMA, and nanoindentation.

Curing Studies. *OAPS/PMDA Nanocomposites.* OAPS was reacted with PMDA to generate tethers that consist exclusively of aromatic rings per Scheme 2. In this network, the estimated tether length is ~1.8 nm (Si−C, ≈0.16 nm; Ph, ≈0.25 nm; Ph−N, ≈0.14 nm; and PMDA imide segment, ≈0.67 nm)[46−49] vs 0.53 nm for the cube body diagonal.[48,49]

Scheme 2. Imide Tether Formation from OAPS and PDMA; Amine/Anhydride = 1

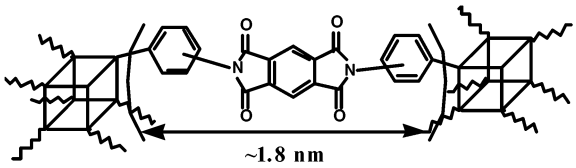

Traditional organic polyimide methods were used with one modification. Because an intermediate OAPS amic acid solution will gel because of cross-linking, the solution must be cast before gelation. PDMA and OAPS were dissolved separately in NMP, mixed at room temperature, and cast immediately onto level glass substrates and dried under N_2. Cure times and temperatures for complete imidization of organic polyimides[33−45,50] were initially used: heating at 60 °C/h to 330 °C under N_2, followed by a 3 h hold at temperature. Although preliminary FTIR studies suggest that these conditions were sufficient to cure the material to >98% sometimes it was necessary to heat at 530 °C/3 h to ensure nearly complete removal of residual defects. Curing of OAPS/PMDA at these temperatures was monitored by FTIR as shown below and as discussed elsewhere.[22]

OAPS/ODPA/ODA Polyimide Nanocomposites. Two separate approaches were taken to introduce some flexibility. First, oxydiphthalic anhydride (ODPA) containing one oxygen link was used in place of PMDA to increase tether flexibility. However, the OAPS/ODPA tether is still short (ODPA imide segment ≈1.2 nm, entire tether ≈2.3 nm)[46,47] and offers cross-link densities similar to those of OAPS/PMDA (3.4×10^{-3} mol/g for OAPS/ODA vs 3.9×10^{-3} mol/g for OAPS/PMDA, number of cross-links equal to 8× mol of cubes).[23] Thus, the network was expected to remain quite stiff.

In a second step, the average tether lengths and cross-link densities were further adjusted by using oxydianiline (ODA). ODA also has one oxygen link, and reaction of ODPA with ODA provides flexible linear imide segments. Therefore, replacing OAPS with ODA in the OAPS/ODPA system generates longer, more flexible tethers consisting of ODPA/ODA and reduces cross-link densities by reducing OAPS loading.

The modified system then consists of OAPS/ODPA with ODA as a diluent. The amine/anhydride ratio (N) was kept at 1 for all formulations, while the OAPS loading fraction was varied from 0 to 100 mol % in increments of 20 mol %. Only linear polyimide forms at 0% OAPS. At the other extreme, 100% OAPS results in maximum cross-link density. These two limiting imide structures are illustrated in Scheme 3.

OAPS/ODPA/ODA nanocomposites were prepared following the same method as for OAPS/PMDA except for 0 mol % OAPS nanocomposites. Note that typical processing of linear imides includes preheating amic

(46) Isaacs, N. S. *Physical Organic Chemistry*; Longman Scientific & Technical: Essex, U.K., 1995; p 32.
(47) Choi, J.; Laine, R. M. unpublished work.
(48) Calzaferri, G.; Marcolli, C.; Imhof, R.; Tornroos, K. W. *J. Chem. Soc., Dalton Trans.* **1996**, 3313.
(49) Auner, N.; Zeimer, B.; Herrschaft, B.; Ziche, W.; John, P.; Weis, J. *Eur. J. Inorg. Chem.* **1999**, 1087.
(50) Takekoshi, T. In *Polyimides*; Ghosh, M. K., Mittal, K. L., Eds.; Marcel Dekker: New York, 1996; p 7.

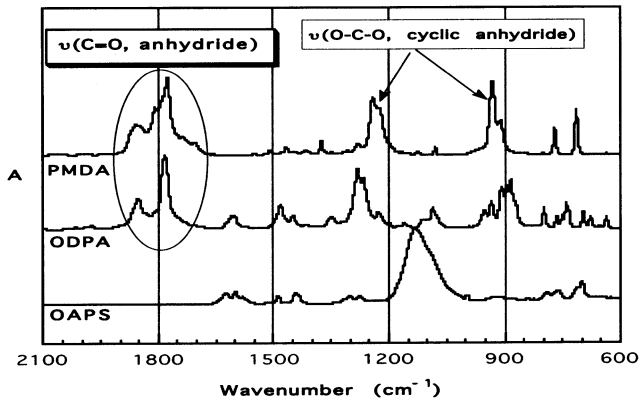

Figure 2. FTIR of OAPS, ODPA, and PMDA. Because characteristic peaks appear at <2000 cm^{-1}, only half of the spectra (up to 2100 cm^{-1}) are shown for ease of comparison.

Scheme 3. Two Imide Extremes: 100% OAPS Offers Maximum Cross-Link Density Whereas 0% OAPS Generates a Linear Thermoplastic Imide[51,52] ($T_g \approx 270$ °C)

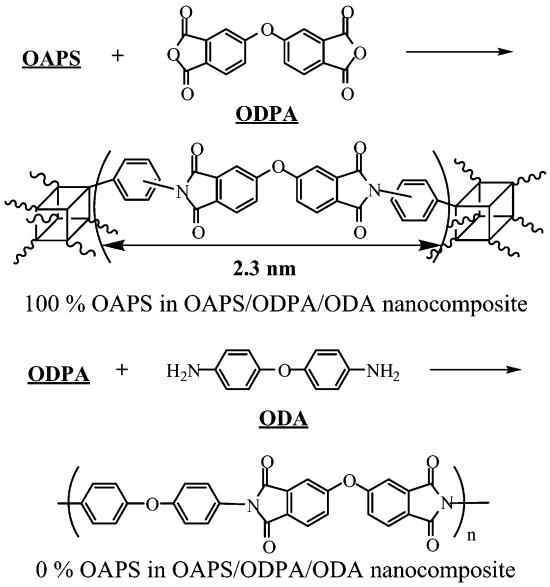

acid solutions to increase the molecular weights to optimize properties. Thus, the 0 mol % OAPS imide was processed by preheating at ≈100 °C for 1 d. For the remaining nanocomposites, amines and anhydride were dissolved separately in NMP to avoid gelation, then mixed and cast immediately on a substrate.

Cure temperatures and OAPS loadings were varied to control the extent of curing and final cross-link density. The resulting composites were recovered as free-standing films on cooling followed by sonication in cold water.

Characterization. *Diffuse Reflectance Fourier Transform Infrared Spectroscopy (DRIFTS).* DRIFTS was used to study the effect of cure temperature on imidization. Spectra of the components were first measured to identify characteristic peaks. These peaks were then used to qualitatively analyze curing within the nanocomposites. Figure 2 shows spectra for OAPS, ODPA, and PMDA. Because characteristic peaks appear at <2000 cm^{-1}, only half of the spectra (up to 2100 cm^{-1}) are shown for ease of comparison.

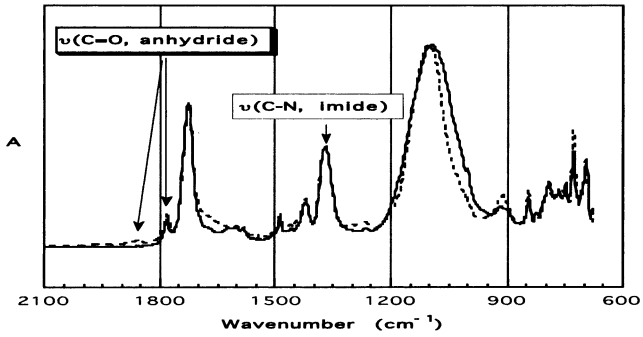

Figure 3. FTIR of OAPS/PMDA cured at 330 °C (- - -) and 530 °C (—).

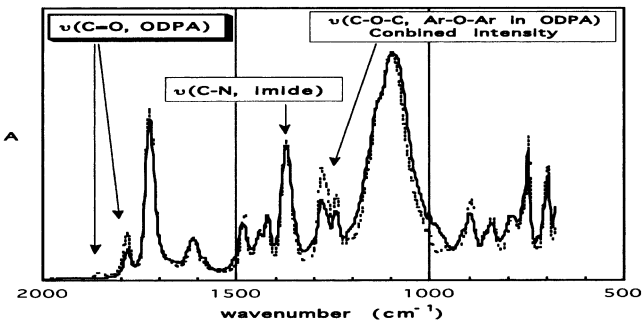

Figure 4. FTIR of 100% OAPS/ODPA cured at 330 °C (- - -) and 530 °C (—). Because characteristic peaks appear at <2000 cm^{-1}, only half of the spectra (up to 2100 cm^{-1}) are shown for ease of comparison.

Several distinct peaks are clearly observed. First, the OAPS spectrum shows a strong υSi−O (cube)[53,54] peak at ≈1100 cm^{-1} which is used as an internal reference for the nanocomposites shown below. Next, both PMDA and ODPA show symmetric and asymmetric υC═O peaks at 1780 and 1850 cm^{-1}, characteristic of cyclic anhydrides.[55] υC−O peaks appear at 950 and 1250 cm^{-1}. The peak at 1250 cm^{-1} for ODPA is an overlay of υC−O of the anhydride and υAr−O in the ODPA backbone. Thus, this peak is expected to remain even after complete imidization.

Once characteristic peaks for the individual nanobuilding blocks and tether components were identified, FTIR spectra of the nanocomposites were obtained using attenuated total reflection IR (ATR). For the OAPS/ODPA/ODA system, the 100 mol % OAPS nanocomposite was used as a baseline spectrum. Figures 3 and 4 show spectra for OAPS/PMDA and OAPS/ODPA cured at 330 °C and 530 °C for 3 h (N_2), respectively.

Although typical imide peaks, e.g., υC−N at 1350 cm^{-1}, and υC═O at 1730 and 1780 cm^{-1}, are clearly visible in both spectra, the changes in peak intensities were hard to quantify. Instead, the anhydride υC═O peaks at 1780 and 1850 cm^{-1} were used for qualitative measurements. Note that some peaks are an overlay of multiple absorptions. For example, the peak at 1780

(51) Ohya, H.; Kudryavtsev, V. V.; Semenoova, S. I. *Polyimide Membranes: Applications, Fabrications and Properties*; Kodansha Ltd: Tokyo, Japan, 1996; p 94.
(52) Sroog, C. E. *Prog. Polym. Sci.* **1991**, *16*, 561.
(53) Marcolli, C.; Calzaferri, G. *Appl. Organomet. Chem.* **1999**, *13*, 213.
(54) Wallace, W. E.; Guttman, C. M.; Antonucci, J. M. *Polymer* **2000**, *41*, 2219.
(55) Silverstein, R. M.; Webster, F. X. *Spectrometric Identification of Organic Compounds*; John Wiley & Sons: New York, 1996; p 71.

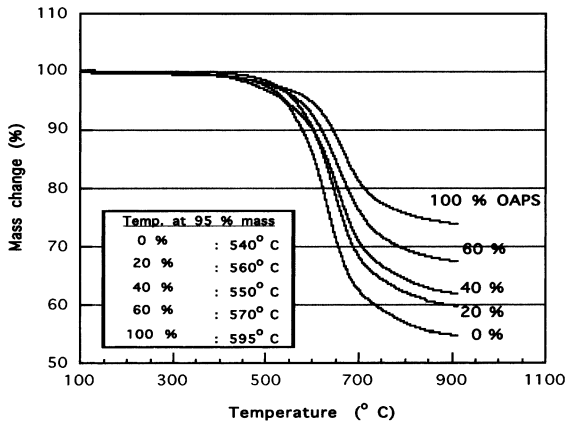

Figure 5. TGA (N_2, 10 °C/min) of OAPS/ODPA/ODA nanocomposites with various OAPS loadings cured at 330 °C.

cm^{-1} combines intensities of $\nu C{=}O$ of the imide and anhydride.

Two features are seen in these FTIR (ATR) spectra. First, although it is reported[50] that imidization is typically complete at temperatures >300 °C, anhydride peaks in this spectrum remain after heating to 330 °C indicating incomplete reaction. This is probably because the increased viscosity on cross-linking and the extreme rigidity of the reactants hinder free access of the functional groups to each other. However, these peaks decrease on heating to 530 °C suggesting that viscosity and the rigidity are mostly overcome and further curing at temperatures >330 °C is necessary. Note that the $\nu C{-}O$ peak for OAPS/PMDA at 1250 cm^{-1} also disappears at 530 °C, but remains for OAPS/ODPA because it is an overlay of two $\nu C{-}O$ bands.

Note that it is possible that the homogeneity of the initial solutions was not complete perhaps because of formation of undetectable colloidal gel particles that might inhibit complete imidization at lower temperatures. Given the rate of gelation, this problem may be resolved by mixing at temperatures lower than room temperature.

Second, peaks broaden slightly at 530 °C suggesting that partial degradation might occur at this temperature. This may be because the residual amine and anhydride groups from the incomplete imidization are susceptible to the thermal degradation. A few percent mass loss at ~530 °C is seen in the TGA of all formulations shown in Figure 5. This suggests slight degradation or perhaps just final loss of water following full imidization. Peak broadening can also be ascribed to the fact that the tethers are highly inflexible, and on full imidization the lack of segment mobility will force tethers into various slightly different conformations, leading to the spectral broadening observed. Such processes could also distort the silsesquioxane core leading to the broadening observed for the $\nu Si{-}O$ bands.

One final comment must be made concerning the potential for ring-opening polymerization (ROP) of the cube core during synthesis of these composites. The imidization reaction does produce some water, which in the presence of high concentrations of base might result in at least partial ROP of the cube core or cleavage of phenyl−Si bonds. Indeed, the reduction of the octanitrophenylsilsesesquioxane using HCO_2H/Et_3N mixtures does lead to formation (10−20% depending on the reaction conditions) of T_2 units in the resulting OAPS.[56a] However, the curing studies are all done in thin films well above the boiling point of water. Hence, diffusion of water out of the thin film is likely to be so rapid as to not offer the opportunity to generate OH^- species that might promote ROP. Second, aminophenyl (aniline) groups are not particularly basic and, as such, the potential for deprotonation is likely to be minimal. Third, curing must proceed via initial formation of amic acid derivatives; thus the overall environment within the film can be expected to become less basic and indeed may offer high microscopic acidities as curing proceeds. Given that the nitro compound is made in fuming nitric acid, we suspect that the potential for ROP after amic acid formation is initiated is reduced rapidly. Finally, as this paper was being revised, a paper by Wright et al. issued discussing the curing of diaminophenyl POSS units with dianhydrides.[56b] These materials were routinely heated to 380 °C without changes in polymer characteristics including the POSS units, again supporting the thermal stability of the aminophenyl cube systems produced here. The fact that FTIR spectral broadening does occur at 550 °C does suggest some modifications to the nanocomposite structure, as discussed above.

Thermogravimetric Analysis (TGA). The thermal stabilities of OAPS/PMDA and OAPS/ODPA/ODA nanocomposites were characterized by TGA. Here, cure temperature and OAPS loading (for OAPS/ODPA/ODA) were varied independently and their effects on initial 5% mass loss temperatures and char yields (1000 °C/N_2) were investigated. Cure times of 3 h were used consistently for all nanocomposites because the DMA properties of OAPS/PMDA did not change after 3 h, suggesting no further changes in cross-link densities.

As expected, the OAPS/PMDA nanocomposite showed excellent thermal stability in air to ~540 °C (TGA not shown). Its 5% mass loss temperature (N_2) is ~600 °C with a char yield of ≈70 wt %. The effect of cure temperature (330° vs 530 °C) was negligible because 5% mass loss temperatures were higher than 530 °C. Char yields do not change either regardless of the cure temperature. This suggests that at higher curing temperatures, curing occurs before unreacted end groups decompose. An alternate interpretation of these results is that the fraction of residual amine and anhydride groups present at ~330 °C is small (e.g., ≪5 wt %). Thus, their effect on the 5% mass loss temperature and char yields should also be negligible. Similar trends are also seen for the OAPS/ODPA/ODA nanocomposites. When cure temperatures were varied, keeping OAPS loading fixed, the effects on 5% mass loss temperatures and char yields were also negligible.

One important interpretation of these results is that pendant reactive groups are sufficiently mobile at higher temperatures to complete the curing process. This may seem somewhat surprising given the rigidity and likely high viscosity of the microscopic environment. However, the high symmetry of the cubes may actually favorably orient the unreacted amic acid components to ensure complete reaction. If this were the case then X-ray

(56) (a) Kim, S. G. and Laine, R. M. unpublished results. (b) Wright, M. E.; Schorzman, D. A.; Feher, F. J.; Jin, R.-Z. *Chem. Mater.* **2003**, *15*, 264.

Table 2. Selected Silica/Polyimide Hybrid Systems with Thermomechanical Properties

ref.	anhydride	amine	silica source	cross-linker	hybrid structure (max. silica loading)	therm. stab. (°C) (T_{onset}, $T_{5\%}$, or T_d)[b]	residues (%) (T > 800 °C)	modulus (GPa)
33	BTDA	ODA	TMOS	DAPrTMDS	I. P. (50 wt %)[c]	~450/~300 (50%)[d] $T_{5\%}$, N_2	10/46 (50%)[d] N_2	–
34	BTDA	BAPS	DEMS	ViPSX	I. P. (50 wt %)	192/100 (50%) T_d, N_2	-	2.6/0.6 (50%)[d]
35	PMDA	ODA	TMOS	APrTMOS	I. P. (55 wt %)	591/542 (55%) $T_{5\%}$, N_2	-	–
36	PMDA	ODA	TEOS	APrTEOS	I. P. (30 wt %)	486/496 (30%) $T_{5\%}$, O_2	0/24.4(30%) O_2	2.1/3.6 (30%)
37	PMDA	PPA MPA	TEOS		500-nm particles[e] (40 wt %)	~550/~600 (40%) $T_{5\%}$, N_2	–	4.0/5.3 (40%)
38	ODPA	DDM APN	P-TEOS		50-nm particles (45 wt %)	444/493 (45%) $T_{5\%}$, N_2	21/44 (45%) N_2	1.8/3.5 (45%)
39	PMDA	DDDM	TEOS		200 nm (5 wt %) 2 μm (20 wt %)	556/582 (20%) T_{onset}, N_2	–	2/4 (40%)
40	BTDA	DDDM	TEOS		300 nm (10 wt %) 2 μm (30 wt %)	509/527 (10%) T_{onset}, N_2	55/65 (10%) N_2	2.2/2.6 (10%)
41	PDMA	ODA	clay[f]		exfoliated (3 wt %)	515/540 (3%) $T_{5\%}$, N_2	–	2.7/5.2 (3%)

[a] Refs 33–40. A clay/polyimide hybrid system is also included for comparison. Ref 41. [b] T_{onset}: degradation onset temperature. $T_{5\%}$: 5% mass loss temperature. T_d: distortion temperature. [c] I. P.: interpenetrating structure. Organic/inorganic phases not distinguishable. [d] A/B (C %): initial property A of pristine polyimide/ changed property B of hybrid at C wt % silica loading. [e] Particles: silica phase separated from polyimide as spherical particles. [f] Clay: montmorillonite.

diffraction powder patterns might be expected to show long-range order associated with periodicity. However, this is not seen for reasons discussed below.

Thus within a given composition cure temperatures >330 °C do not significantly affect the thermal stability of the nanocomposite. Therefore, a standard cure temperature of 330 °C was instituted for our studies. In contrast, the OAPS loading does significantly affect thermal stability as seen in the Figure 5 TGA results.

As the OAPS loading increases from 0 to 100 mol %, the 5% mass loss temperatures increase by ≈50 °C. In air, the 100% OAPS composite gives ceramic yields (1000 °C) of ≈20 wt % (as SiO_2), which is theoretical, while at 0% OAPS, the imide oxidizes completely. Second, the char yields (N_2) also increase from 55 to 75% at 100 mol % OAPS loading. Even for 60% loading, the char yield is over 65%. Thus, it appears that imide components give ≈50% char yields, and silica components in OAPS increase char yields quantitatively up to an additional 20%. High char yields are a direct indication of resistance to combustion. Preliminary studies on resistance to degradation by O atoms shows improvements over normal polyimides such as Kapton.[57] Indeed, preliminary measurements indicate that the OAPS/PMDA materials are at least comparable to other POSS composites which out perform Kapton.[57c]

Off-stoichiometry nanocomposites (e.g., 5% more OAPS than dianhydride or vice versa) exhibit decreases in 5% mass loss temperatures and char yields to 520 °C (vs 600 °C) and ~68 wt % (vs 75 wt %), respectively. This is certainly because unreacted pendant groups decompose before the imide tethers. A similar trend is also expected and observed for epoxy cube nanocomposites.[17,18,22,23] These results support our argument above that suggests that imidization occurs more readily than defect decomposition processes.

These results also indicate that the imide tethers control nanocomposite thermal stabilities. Indeed FTIRs of the 550 °C cured materials show that the cube structure remains intact.[22] Likewise, they must also control the thermomechanical properties. These observations compare with those of silica-filled polyimides.

Polyimides are typically reinforced with silica via in-situ sol–gel methods to minimize phase segregation for optimal mechanical properties; condensation of alkoxysilane and imidization often proceed concurrently. The use of organic/inorganic phase cross-linkers consisting of both alkoxysilane and amine usually produces hybrids homogeneous at a molecular level.[33–36] When cross-linkers are not used, the resulting silica particle sizes range from 50 nm to 1–2 μm and increase with increasing silica loadings (to ≈50 wt % vs ≈20 wt % silica for OAPS/PMDA and OAPS/ODPA).[37–40] Table 2 shows selected silica/polyimide hybrid systems with thermomechanical properties.[33–40] A representative clay/polyimide hybrid system is also included for comparison.[41]

Materials. Abbreviations used are as follows: BTDA, 3,3′,4,4′-benzophenone tetracarboxylic dianhydride; ODA, oxydianiline; TMOS, tetramethoxysilane; DAPrTMDS. diaminopropyl tetramethyldisiloxane; BAPS, 2,2-bis[4-(3-aminophenoxy)phenyl]sulfone; DEMS, diethoxymethylsilane; ViPSX, vinyl-containing diaminopolysiloxane; PMDA, pyromellitic dianhydride; APrTMOS, 3-aminopropyltrimethoxysilane; TEOS, tetramethoxysilane; APrTEOS, 3-aminopropyl)triethoxysilane; PPA, *p*-phenylene diamine; MPA, *m*-phenylene diamine; ODPA, 4,4′-oxydiphthalic anhydride; DDM, 3,3′-diaminodiphenylmethane; APN, 4-aminophenol; P-TEOS, phenyltriethoxysilane; DDDM, 4,4′-diamino-3,3′-dimethyldiphenylmethane.

Thermal stabilities for the hybrids reported here are better than those for pristine polyimides. For example, 5% mass loss temperatures can increase by up to 50 °C.[37,38] However, some silica/imide hybrids often exhibit significant mass losses (≈5 wt %) at temperatures <400 °C because condensation reactions proceed further on heating beyond imidization temperatures (~300 °C) and give off water.[33–35] Char yields usually increase in proportion to the silica loadings. Unfortunately, the

(57) (a) Gilman, J. W.; Schlitzere, D. S.; Lichtenhan, J. D. *J. Appl. Polm. Sci.* **1996**, *60*, 591. (b) Gonzalez, R. I.; Phillips, S. H.; Hoflund, G. B. *J. Spacecraft and Rockets* **2000B**, *37*, 463. (c) Gonzalez, R. I. private communication.

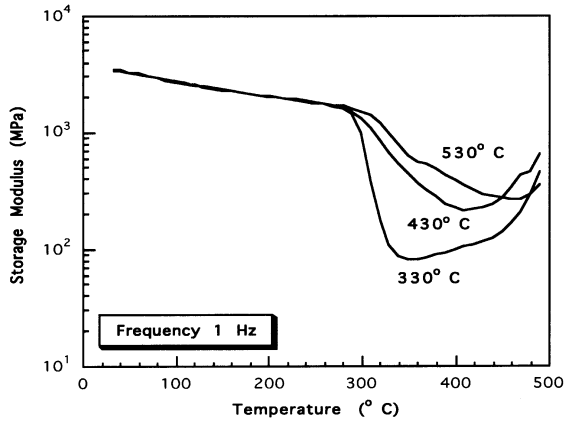

Figure 6. Storage modulus of 20 mol % OAPS/ODPA/ODA nanocomposites cured at selected temperatures, 3 h, N_2.

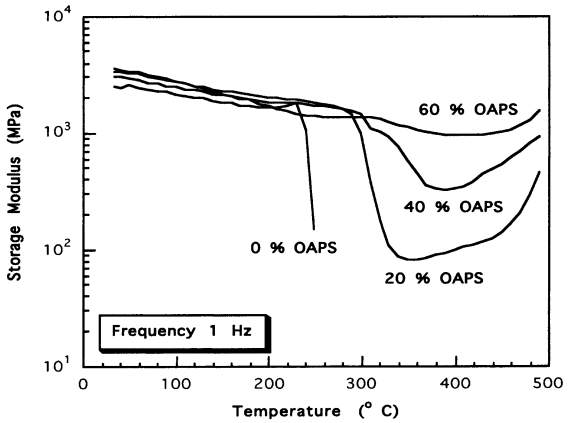

Figure 7. Storage moduli of nanocomposites cured at 330 °C at selected OAPS loadings.

extensive difference in processing methods, variables, and chemical components does not allow a simple comparison between the Table 2 list of composites and the cube nanocomposites discussed here, but see below.

Dynamic Mechanical Analysis (DMA). Nanocomposite thermomechanical properties were characterized using DMA. Although the OAPS/PMDA nanocomposites are thermally stable, the fully cross-linked films are so brittle they do not survive the tensile stresses arising from the volume shrinkage during the imidization process and fracture extensively. No reliable mechanical properties measurements were possible by DMA or nanoindentation. In comparison, the stiffness of OAPS/ODPA/ODA nanocomposites can be adjusted by changing the OAPS loadings. Thus, the mechanical properties discussed below are limited to the OAPS/ODPA/ODA system.

A set of model curing studies was conducted using the OAPS/ODPA/ODA system with 20 mol % OAPS. The lowest cure temperature tested was 330 °C following the cure conditions for the organic polyimide.[33−45,50] At temperatures ∼200 °C, the resulting nanocomposites were unstable due to incomplete imidization. Cure times of 3 h were sufficient to obtain reproducible DMA results and thus were used for all nanocomposites.

As seen in Figure 6, the baseline rubbery state modulus at 20 mol % OAPS (lowest OAPS loading tested) cured at 330 °C was low due to the low cross-link density, and further increases in rubbery modulus were observed at higher temperatures suggesting further imidization. Figure 6 shows that the storage modulus profiles for materials cured at 330, 430, or 530 °C also improved on heating above the original cure temperature. This points to incomplete imidization even at 530 °C, as suggested by the FTIR studies above. Thus optimal processing for these materials can require temperatures of >500 °C, which is normally quite high for standard polymer processing methods.

Another variable in thermoset cube nanocomposite design is control of cross-link densities. Because each cube offers eight cross-links localized in a small volume (phenyl cube diameter ∼1.3 nm), cube loading offers a simple way to vary the cross-link densities. As noted above, cooperative motions of multiple tethers are likely very limited and individual tether relaxation motion should dominate global relaxation. In the very rigid systems created here, tether motions are expected to be marginal. Again, this assumes that all of each functional group on each cube reacts equally.

As more OAPS is used instead of ODA, the average tether length is reduced and the cross-link density increases. Simultaneously, most tether relaxation motions are reduced or eliminated. Conversely, the rubbery state moduli increase as demonstrated in Figure 7.

Figure 7 compares the storage moduli of OAPS/ODPA/ODA nanocomposites with various OAPS loadings up to 60 mol %. Nanocomposites with 100 mol % OAPS loadings could not be tested by DMA because the resulting highly cross-linked materials do not survive the volume shrinkage that occurs during imidization, resulting in wrinkled films with multiple cracks. Thus, the mechanical properties of these materials were characterized by nanoindentation as described below. Note that no rubbery state moduli can be measured for 0 mol % OAPS imide because the linear chains relax completely at temperatures $> T_g$ in this case. The T_g of 0% OAPS imide measured by DMA was ≈270 °C, same as the literature value.[51,52]

Comparison of these profiles shows that as the OAPS content increases, relaxation motions within the network diminish and the distinction between the glassy and rubbery states becomes ambiguous with only small decreases in moduli. This is particularly true for 60 mol % OAPS loading where no decrease in modulus is observed. Furthermore, the onset temperature for relaxation increases immediately by ∼60 °C on going from 0 to 20 mol % OAPS.

In general, individual profiles exhibit increases in rubbery state moduli at temperatures greater than the 330 °C cure temperature. However, this change becomes insignificant at 60 mol % OAPS loading likely because the network is so highly cross-linked that even heating to >330 °C cannot further improve the properties. Thus, increases in OAPS content, which increase cross-link density, also reduce the optimal curing temperature while also increasing the overall elastic moduli, which would be expected for materials with higher overall cross-link densities.

Nanoindentation. Generally, DMA is not suitable for precise measurement of thin film moduli primarily because of the errors associated with film thickness, e.g., ∼30 μm is difficult to measure precisely. Our DMA measurements also produced inconsistent room-temperature moduli, in particular for the higher cross-link

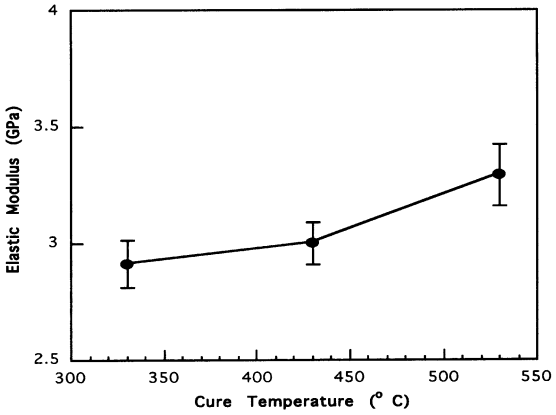

Figure 8. Modulus of 20% OAPS/ODPA/ODA nanocomposites measured by nanoindentation.

density materials. Thus, we sought an alternate method of measuring the modulus more precisely.

Nanoindentation offers a complementary method of measuring elastic moduli because this technique measures surface moduli using penetration depths of only nanometers.[58] It also provides a reliable measure of a sample's compressive properties. Furthermore, nanoindentation can be used for brittle films that cannot be tested by DMA. The commercial epoxy resin prepared by reacting the diglycidyl ether of bisphenol A (DGEBA) with diaminodiphenylmethane (DDM) was used to generate reference values. Nanoindentation provides a modulus of 2.8 GPa vs 2.4 GPa measured by tensile testing.[17,18]

For this study, a 300-nm penetration depth was used. Thus, it appears that nanoindentation can measure the moduli within a ≈15% error range. In comparison, the literature suggests errors of ∼5% in measuring moduli by nanoindentation.[58]

Figure 8 shows nanoindentation elastic moduli for 20% OAPS/ODPA/ODA nanocomposites at various cure temperatures (3 h, N_2). All data represent an average of five measurements. These elastic moduli range from 2.9 to 3.3 GPa for all samples. In comparison, the literature tensile modulus is 2.2 GPa for ODPA/ODA[59] and 1.8−2.9 GPa for PDMA/ODA.[36,41,42] Nanoindentation moduli for linear PDMA/ODA are reported as 2.2−2.5 Gpa[60,61] whereas that of cross-linked PDMA/ODA is 3.0−3.4 GPa.[61] Thus, 3 GPa is a reasonable value for the cross-linked 20% OAPS/ODPA/ODA network.

Note that for this system, the cure temperature has only a modest effect on modulus, increasing only ∼10% at 530 °C. Note that nanoindentation measures moduli in compression. Thus, these results suggest that the majority of the imide tethers form on curing at temperatures >300 °C and extra cross-linking by curing at higher temperature does not affect compressive moduli significantly. However, "tensile" mode DMA tests clearly show increases in cross-link densities and rubbery state moduli as discussed above, suggesting that tensile moduli are more sensitive to cross-link densities than compression moduli. Unfortunately, no literature was found for the effects of cure temperatures >300 °C on mechanical properties of organic polyimides, probably because imidization is normally complete at ≈300 °C.

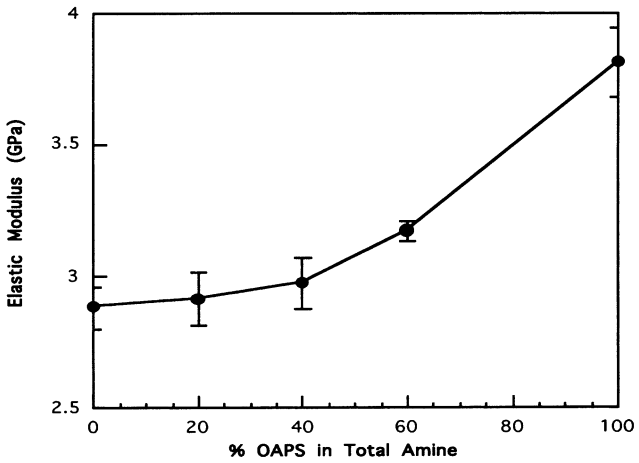

Figure 9. Compressive moduli of OAPS/ODPA/ODA (cured at 330 °C, 3 h, N_2) nanocomposites at selected OAPS loadings as measured by nanoindentation.

In comparison, nonlinear increases in moduli were found when the cross-link density was varied by changing the cube loading. Figure 9 shows the moduli of OAPS/OD-PA/ODA nanocomposites with various OAPS loadings cured at 330 °C for 3 h. In this test, moduli remain at ∼3 GPa until ∼50 mol % OAPS loadings and then increase to 3.8 GPa at 100 mol % OAPS loading. Note that net silica loading for OAPS/ODPA/ODA is ∼20 wt % at 100 mol % OAPS. In comparison, elastic moduli of silica-filled polyimides usually increase (up to ∼100%) in proportion to silica loadings to ∼40 wt % (see Table 2). However, soft hybrids with poor moduli also result when imidization/condensation are not complete.[34] Literature compression moduli were unavailable for aromatic polyimides.

These results suggest that nanoindentation moduli arise mostly from the much higher cross-link densities, which is not unexpected because higher cross-link densities should greatly increase stiffness. The effects of tether relaxation motions are likely small as the moduli remain at ∼3 GPa at OAPS loadings from 0 to ∼ 60 mol % where changes in global relaxation were clearly observed in DMA tests.

Selected Comments. Given the above characterization data, some observations about the nanostructure of these materials must be made. We begin with X-ray powder pattern studies (Figure 10) which suggest that for all compositions of OAPS/ODPA no long-range ordering results during the cross-linking process. The observed powder pattern for OAPS (OAPhS in Figure 10) shows only one clear peak at ≈8° 2θ which corresponds roughly to the diameter of the octaphenylsilsesquioxane core (1−1.1 nm). The only other peak appears to be that at ≈20° 2θ which is typical for an amorphous material. Given that the starting OPS is highly crystalline, we presume that the transformation to an amorphous material arises because of the substitution pattern at the phenyl groups which produces an *m*/*o*/*p* ratio of roughly 60:30:10. Consequently, packing at the molecular level can be expected to be haphazard, reducing the opportunity for a high degree of periodicity.

(58) Oliver, W. C.; Pharr, G. M. *J. Mater. Res.* **1992**, *7*, 1564.
(59) Tsai, M.; Whang, W. *J. Appl. Polym. Sci.* **2001**, *81*, 2500.
(60) Dabral, M.; Xia, X.; Gerberich, W. W.; Francis, L. F.; Scriven, L. E. *J. Polym. Sci. Part B: Polym. Phys.* **2001**, *39*, 1824.
(61) Tsai, F.-Y.; Alfonso, E. L.; Harding, D. R.; Chen, S. H. *J. Phys. D.: Appl. Phys.* **2001**, 34, 3011.

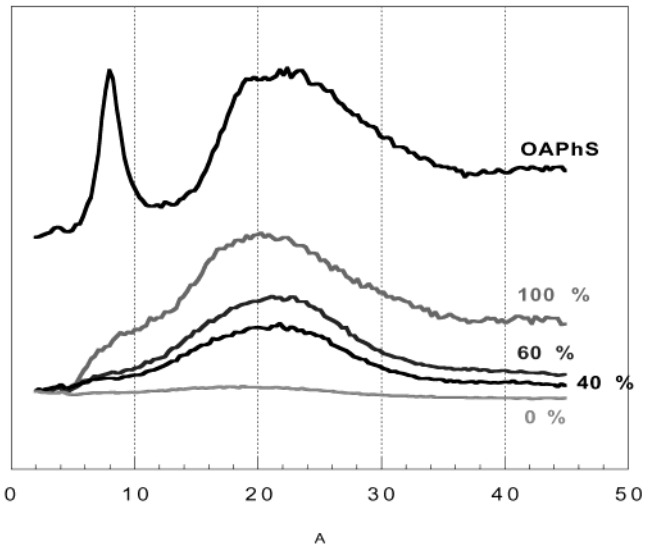

Figure 10. XRD powder patterns of OAPS/ODPA/ODA (cured at 330 °C, 3 h, N_2) nanocomposites at selected OAPS loadings and of pure OAPS (OAPhS).

On this basis, we can assume that the opportunity to form highly periodic polyimide structures that would produce discernible peaks in XRD diffraction patterns is likewise diminished. Only the 100% OAPS/ODA nanocomposite shows some hints of a periodic structure suggested by a shoulder at 8−10° 2θ.

These results are contrasted by the FTIR data above (Figures 3 and 4) that suggest that only residual amounts of anhydride remain unreacted in fully cured OAPS/PMDA and OAPS/ODA nanocomposites. This implies that the imidization process is nearly complete despite (a) the expected high viscosity during imidization, (b) the presence of significant amounts of ortho substitution which might be expected to be relatively inaccessible especially toward completion of the imidization process, and (c) the fact that these materials gel easily which again might be expected to inhibit complete imidization.

On the basis of these observations, it can be argued that because the nanostructures are highly regular, imidization is geometrically favored despite all the potential obstructions to the process. If imidization is favored geometrically, one might expect the highly rigid 100% OAPS/ODA material with a 2.3-nm tether to exhibit well-defined nanoporosity as we have observed in other instances.[20] However, all efforts to detect nanoporosity using BET measurements in our laboratories and at Micromeritics Inc. were unsuccessful.

Thus, either these materials lack any porosity or the pores present do not desorb gases at rates measurable by standard porosimetry studies. Positron annihilation studies offer the potential to resolve these problems as done earlier.[20]

In our previous work on OAPS/PMDA, the resulting materials were too brittle to prepare specimens for characterization by standard mechanical testing methods. However, in the current studies even at OAPS/ODA 100% compositions we were able to make materials that could be tested at least with nanoindentation. In principle, it may be that following the imidization process, OAPS/PMDA cross-link densities are so high that the levels of stress at nanometer length scales actually promote propagation of cracks. Furthermore, the absence of tether flexibility would suggest that there is no way to anneal these stresses out of the OAPS/PMDA nanocomposites, whereas in the OAPS/ODA system some limited flexibility exists allowing relief of imidization-induced stress. We hope to model these systems soon to determine if this perspective is realistic.

As noted above, these materials offer good to excellent thermal stabilities, on the order of those expected for simple polyimides. However, one key aspect here is that most well-known polyimides are highly linear, whereas the current systems are highly cross-linked. This leads to excellent compressive moduli, in contrast to most polyimide systems which are known to exhibit excellent tensile properties but to behave very poorly under compression. In principle it may be possible to produce polyarimid fibers based on OAPS that offer both good tensile and compressive properties, providing a way can be developed to spin these highly cross-linkable systems. Thus, one future goal of this work is to develop melt spinnable precursors.

Conclusions

This study demonstrates several characteristics of imide cube nanocomposites. First, imide cube nanocomposites can be prepared by a simple one-step casting-curing process. Compared with other polyimide−inorganic hybrid composites typically prepared carefully via sol−gel reaction or physical blending, hybridization using OAPS is remarkably simple but still guarantees a uniform distribution of inorganic components within the matrix imide. This process is even simpler than the traditional method of processing organic polyimides because no step for preheating amic acid is necessary.

Second, it is relatively easy to tailor the network structure segment by segment; tether structures can be varied by adjusting the anhydride structure and tether lengths can be controlled by addition of an amine diluent. Manipulation of the tether segments also provides control of the nanocomposites processability and thermomechanical properties.

Third, cubes improve network thermomechanical stabilities via cross-linking and “perfect silica particle dispersion.” In cube nanocomposites, cooperative relaxation of multiple tethers is limited and individual tether segmental motions dominate macroscopic relaxation at elevated temperatures. Because imide tethers are rigid, cross-linking easily reduces their segmental, and thus macroscopic, relaxation. In general this should lead to very brittle structures, but the opportunity to selectively modify the tether suggests many ways to improve toughness and compressive strength without sacrificing global properties.

An alternate perspective on the “brittle” nature of these materials comes from the fact that ceramics are brittle materials but are readily processed into high performance ceramic fibers and films that do not suffer catastrophic failure because the energy required to initiate cracks and propagate cracks increases greatly as structural dimensions drop below 20 μm. Hence, the opportunity exists to make high-strength fibers from these materials. The best approach would be to develop a melt processing method.

Finally, this study also demonstrates that OAPS can serve as a versatile platform from which various organic tethers can be derived. Imide tethers are just one example. In general, any polymer structure derivable from amine such as an amide could be constructed from OAPS offering numerous opportunities to develop novel composites.

Acknowledgment. We thank the FAA, AFOSR, Matsushita Electric Inc., and Guardian Industries for partial support of the work reported here. Finally, we thank Professor V. Kennedy of Eastern Michigan University for a careful reading of this manuscript.

CM030286H